



Effects of biomass-burning-derived aerosols on precipitation and clouds in the Amazon Basin: a satellite-based empirical study

J. C. Lin,^{1,2} T. Matsui,¹ R. A. Pielke Sr.,¹ and C. Kummerow¹

Received 12 November 2005; revised 13 February 2006; accepted 29 June 2006; published 12 October 2006.

[1] Biomass burning in the Amazon provides strong input of aerosols into the atmosphere, with potential effects on precipitation, cloud properties, and radiative balance. However, few studies to date have systematically examined these effects at the scale of the Amazon Basin, over an entire burning season, using available data sets. We empirically study the relationships of aerosol optical depth (τ_a) versus rainfall and cloud properties measured from satellites over the entire Brazilian Amazon during the dry, biomass burning seasons (August–October) of 2000 and 2003. Elevated τ_a was associated with increased rainfall in both 2000 and 2003. With enhanced τ_a , cloud cover increased significantly, and cloud top temperature/pressure decreased, suggesting higher cloud tops. The cloud droplet effective radius (R_e) exhibited minimal growth with cloud height under background levels of τ_a , while distinct increases in R_e at cloud top temperatures below -10°C , indicative of ice formation, were observed with aerosol loading. Although empirical correlations do not unequivocally establish the causal link from aerosols, these results are consistent with previous observational and modeling studies that pointed to dynamical effects from aerosols that invigorate convection, leading to higher clouds, enhanced cloud cover, and stronger rainfall. We speculate that changes in precipitation and cloud properties associated with aerosol loading observed in this study could have important radiative and hydrological effects on the Amazonian climate system. The accelerated forest burning for agricultural land clearing and the resulting enhancements in aerosols and rainfall may even partially account for the observed positive trend in Amazonian precipitation over the past several decades.

Citation: Lin, J. C., T. Matsui, R. A. Pielke Sr., and C. Kummerow (2006), Effects of biomass-burning-derived aerosols on precipitation and clouds in the Amazon Basin: a satellite-based empirical study, *J. Geophys. Res.*, *111*, D19204, doi:10.1029/2005JD006884.

1. Introduction

[2] Forest fires in the Amazon, which have accelerated over the past decades because of human activities [Crutzen and Andreae, 1990; Setzer et al., 1994], release large quantities of aerosols into the atmosphere. Aerosols serve as cloud condensation nuclei (CCN) [Warner and Twomey, 1967], modifying cloud properties and affecting the climate system [National Research Council (NRC), 2005; Ramanathan et al., 2001]. Enhanced input of aerosols into the atmosphere has been suggested to suppress precipitation [Ramanathan et al., 2001] by increasing CCN concentrations and reducing cloud droplet size and droplet coalescence [Twomey, 1977]. Changes in tropical precipitation can have significant, potentially even global consequences. Tropical precipitation provides three fourths of the energy that drives the atmospheric wind circulation through latent

heat release [Kummerow et al., 2000]. A significant fraction of tropical precipitation takes place in Amazônia [Chahine, 1992], which is the largest expanse of tropical rain forest in the world [Food and Agriculture Organization, 1993]. Suppression of rainfall can potentially lead to a positive feedback through a drier land surface, stronger susceptibility to fires, and even greater aerosol-induced suppression of rainfall [Laurance and Williamson, 2001]. Such perturbations to the hydrological cycle can also have major consequences for the fresh water supply [Lohmann and Feichter, 2005; Ramanathan et al., 2001].

[3] Rosenfeld [1999], using satellite-based precipitation observations from the Tropical Rainfall Measuring Mission (TRMM), illustrated for a single day that aerosols from a biomass burning event in Indonesia shut down warm-rain processes. Kaufman and Fraser [1997], on the basis of satellite observations from the AVHRR sensor, have shown a reduction in the cloud droplet radius with aerosol loading from biomass burning in the Amazon but did not quantify the effect on precipitation. Andreae et al. [2004], analyzing aircraft observations in the Amazon, found reductions in cloud droplet sizes and delays in the onset of precipitation within smoky clouds. The lack of early warm-rain processes enabled updrafts to accelerate and reach higher altitudes and produce stronger

¹Department of Atmospheric Science, Colorado State University, Fort Collins, Colorado, USA.

²Now at Department of Earth Sciences, University of Waterloo, Waterloo, Ontario, Canada.

storms. Thus the authors concluded that the net effect of aerosols on total precipitation “remains unknown.”

[4] Furthermore, aerosol-induced modification of cloud properties which cause changes in precipitation can also have radiative consequences. *Twomey* [1977] pointed out that the increase in droplet concentrations and decrease in droplet size from aerosol loading cause clouds to be more reflective, given a constant liquid water path. *Albrecht* [1989] suggested that aerosol-induced drizzle reduction increases the cloud cover, enhances global albedo, and cools the Earth’s surface. Nonetheless, the exact radiative effect of clouds depends critically not just on amount and droplet concentrations, but also on the phase of hydrometeors and the height of clouds [*Intergovernmental Panel on Climate Change (IPCC)*, 2001b; *NRC*, 2005]. How biomass burning aerosols affect ice formation and cloud height remains a key question that needs to be examined.

[5] *Sekiguchi et al.* [2003] investigated global-scale correlations between low-level cloud properties and aerosol concentrations measured by AVHRR sensor over the ocean. They reported increased cloud fraction with enhanced aerosols but no clear relationship with cloud top temperature. The emphasis on oceanic measurements and the global scope of this study precluded clear conclusions about the effects of Amazonian biomass burning. *Koren et al.* [2004], using MODIS measurements on the Aqua satellite, found scattered cumulus cloud cover in the Amazon to decrease with increases in biomass-burning-derived aerosols. They did not report the effect on the total cloud cover or other cloud properties.

[6] Given the inconclusive nature and the limited spatial/temporal coverage in previous studies, we examine data from satellites that sample extensively in both the spatial and temporal domains, focusing on Amazônia. We include all clouds detected from the satellite sensors, rather than restricting the analyses to low-level clouds or as in past studies. Amazonian cloud cover is characterized by scattered cumuli in the lower levels [*Koren et al.*, 2004] and strongly convective clouds that reach higher altitudes [*Hartmann*, 1994], instead of stratus layers more typical of marine clouds.

[7] The analysis combines satellite observations of precipitation from the two sensors in the TRMM mission [*Simpson et al.*, 1996] and measurements of aerosol optical depth (τ_a) [*Kaufman et al.*, 1997] as well as cloud properties [*Platnick et al.*, 2003] from the MODIS sensor on board the Terra platform.

[8] We attempt to address the following question: What is the quantitative effect of biomass burning derived aerosols on precipitation and clouds over the Amazon Basin during the dry season? The study adopts an empirical approach, examining relationships between τ_a and other variables. While the approach cannot unequivocally establish the effects of aerosol loading in a mechanistic way, we envision this work as a first determination of observed relationships that can be probed in future studies (e.g., using models).

2. Study Region

[9] The study region is shown as the red box in Figure 1. This region is primarily covered by the tropical rain forest, excluding the savanna region in southern Brazil, and over-

laps to a great extent with a previous study in the Amazon [*Koren et al.*, 2004]. Because of the small number of large cities in the study region, the dominant source of aerosols is biomass burning, particularly during the dry season (August–October) [*Guyon et al.*, 2003; *Procopio et al.*, 2004]. The mean τ_a averaged over August–October of 2000 (Figure 1) shows elevated values of over 0.4 across a broad region of the Amazon, from Ji-Parana in the southwest all the way to Santarém and Manaus in the north.

3. Data Sets Used

[10] The following data sets cover the peak of the dry season (August–October) from 2 years: 2000 and 2003. Focusing solely on the dry season ensures large signals of aerosol loading from biomass burning and reduces potentially confounding effects from seasonal variability.

3.1. TRMM Microwave Imager (TMI) and Precipitation Radar (PR)

[11] The TMI measures radiation at five microwave frequencies: 10.7, 19.4, 21.3, 37, 85.5 GHz, with a 760 km swath and footprints ranging from 63 km \times 37 km at 10.7 GHz to 7 km \times 5 km at 85.5 GHz [*Kummerow et al.*, 2000]. The retrieval method for precipitation and vertical hydrometeor profiles is a Bayesian inverse method that varies a priori hydrometeor profiles from a look-up table generated by a cloud resolving model (see details given by *Kummerow et al.* [1996]).

[12] Comparisons of retrieved values with validation data have shown the performance to be better over the ocean, where the low emissivities ($\varepsilon \sim 0.5$) provide a cold background that is clearly contrasted from the radiation [*Kummerow et al.*, 1996]. The high emissivities ($\varepsilon \sim 0.9$) of land surfaces create a warmer background that obscures the hydrometeor signal. However, radiation at the higher frequency 85.5 GHz channel is strongly scattered by ice, thereby lowering the brightness temperature and enabling a measure of the integrated ice content.

[13] PR is the first radar instrument designed to monitor rainfall from space [*Kummerow et al.*, 2000]. It measures the radar echo at a single frequency (13.8 GHz). PR has a subsatellite footprint of 250 m vertically by 4 km horizontally, over a 215 km swath [*Kummerow et al.*, 2000]. The description of the retrieval algorithm is given by *Iguchi et al.* [2000].

[14] The PR precipitation product, as well as the TMI product, have been compared to ground-based rain gauge measurements in, e.g., West Africa [*Nicholson et al.*, 2003]. From this comparison the RMS errors for PR and TMI for seasonal rainfall (aggregated to 2.5° \times 2.5°) were 1.6 mm/day and 1.9 mm/day, respectively. Because of limited number of rain gauge observations in the Amazon no such quantitative evaluations of TRMM rainfall estimates in this region have been carried out at the basin scale.

[15] For this study we used the TRMM 3G68Land product, which grids the level-2 TMI (2A12) and PR data (2A25) into 0.1° \times 0.1° cells.

3.2. MODIS Aerosol Optical Depth (τ_a)

[16] MODIS (Moderate Resolution Imaging Spectroradiometer) has 36 channels, ranging in wavelength from 0.4 μ m

Spatial Distribution of Average MODIS Aerosol Optical Depth during Aug~Oct 2000

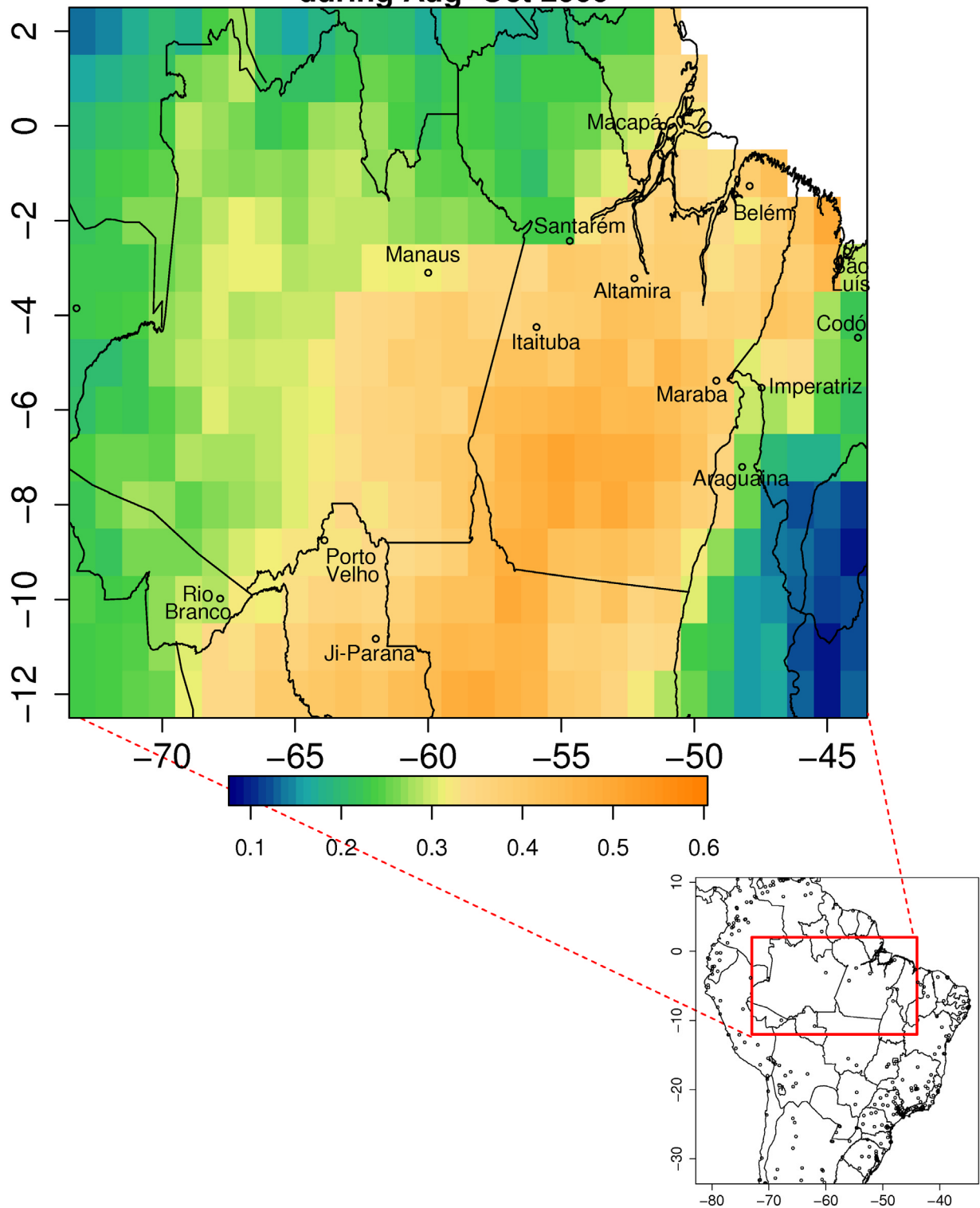


Figure 1. Mean spatial distribution of MODIS aerosol optical depth at 0.55 μm during August–October 2000, over the study domain in this paper (red box). Major cities with total population greater than 100,000 are also shown.

to 14.4 μm . It makes possible unprecedented satellite-based monitoring of τ_a and aerosol properties. For the first time, the MODIS measurements enabled global, operational retrieval of τ_a over land [Kaufman and Tanre, 1998]. The MODIS retrieval method for τ_a is described by Kaufman et al. [1997], and a comprehensive description of MODIS aerosol products is given by Remer et al. [2005].

[17] The MODIS aerosol optical depth retrievals have been extensively validated against a ground-based network of Sun photometer sensors (AERONET), showing that the retrievals were found within $\Delta\tau_a = \pm 0.05 \pm 0.2\tau_a$ [Chu et al., 2002].

[18] For this study we used the level-2 product of τ_a at 0.55 μm and at 10 km \times 10 km footprint on board the Terra satellite (MOD04_L2, Collection 4). Terra flies in a sun-synchronous orbit with a 1030 LT hour equatorial crossing time.

3.3. MODIS Clouds

[19] The cloud fraction is produced by the 1 km \times 1 km footprint MODIS cloud mask (MOD35_L2, Collection 4) algorithm, which makes use of as many as 14 of the 36 MODIS spectral bands to identify clouds [Ackerman et al., 1998, 2002]. The cloud mask “essentially assesses the likelihood of a pixel being obstructed by clouds” and is clear-sky conservative, in that a high probability is necessary for a pixel to be classified as cloudy [Platnick et al., 2003, p. 461].

[20] The following MODIS-Terra cloud variables derive from the MOD06_L2, Collection 4 product. The cloud top pressure/temperature and cloud phase are at 5 km \times 5 km footprint, while the cloud microphysical properties (cloud droplet effective radius (R_e) and water path (WP)) are at 1 km \times 1 km footprint.

[21] The cloud top pressure and temperature retrieval follows the “radiance ratio method” [Kidder and Vonder Haar, 1995], in which ratios between measured radiances at two different frequencies close to one another can be related to the cloud top pressure [Menzel et al., 2002]. The specific method adopted in MODIS makes use of the CO₂ slicing technique that examines the different radiances in the numerous MODIS infrared bands found within the broad 15- μm CO₂ absorption region [Platnick et al., 2003].

[22] The cloud phase retrieval is based on the bispectral infrared algorithm that relies upon the contrasting effects of water droplets and ice crystals on the brightness temperature differences at the 8.52- and 11- μm bands [Platnick et al., 2003]. The “ice cloud coverage” used in this study is defined as the percentage of 5 km \times 5 km pixels classified in the ice phase.

[23] R_e and the cloud optical thickness (τ_c) are retrieved from combining the MODIS water-absorbing bands (1.6, 2.1, 3.7 μm) along with a nonabsorbing band (0.65 μm for over land) [Platnick et al., 2003]. The water path (WP) (the atmospheric column-integrated amount of liquid or ice water) simply follows from the product of τ_c and R_e as $WP = 2\rho\tau_c R_e/3$ [King et al., 1997], where ρ is the density of water. This algorithm assumes that R_e represents the column averaged values. However, R_e retrieved from the visible/infrared wavelengths tends to reflect values near cloud-top because of the strong cloud absorption in the infrared band. While WP could be overestimated/underestimated depend-

ing on the actual profile of R_e , Platnick [2000] has shown this error to be small.

[24] We removed potential artifacts in the cloud properties versus τ_a relationship due to aerosol contamination in the cloud mask algorithm [Brennan et al., 2005]. The cloud mask product includes an aerosol bit as an indicator of potential aerosol contamination [Ackerman et al., 2002]. Pixels with the aerosol bit set to true were removed from calculation of cloud fraction, R_e , and WP .

3.4. NCEP/NCAR Reanalysis

[25] The NCEP/NCAR Reanalysis [Kalnay et al., 1996] is a multidecadal record of atmospheric variables (2.5° \times 2.5°, 6 hourly) generated by assimilating observations using an atmospheric model. The same atmospheric model and data assimilation system, based on the three-dimensional variational (3DVAR) method, are used throughout the record to avoid spurious jumps in atmospheric state variables.

[26] As one of the few available assimilated data sets of the global atmosphere, the NCEP/NCAR Reanalysis was used in this study to account for synoptic-scale forcing of buoyancy generation and precipitation and to separate such influences from aerosol effects. We compared the vertically integrated moisture flux convergence and the cloud work function (CWF) from the Reanalysis fields and found CWF to correlate more strongly with observed precipitation and cloud properties. CWF was first introduced by Arakawa and Schubert [1974] as a measure of the total buoyancy force in clouds. The Reanalysis adopted a simplified Arakawa-Schubert convective parameterization [Kalnay et al., 1996] that retains the CWF as a trigger for convection but considers only a single cloud type, rather than a spectrum of clouds [Pan and Wu, 1995]. The CWF is identical to the commonly used convective available potential energy (CAPE) but also accounts for the effect of entrainment in reducing buoyancy [Emanuel, 1994; Pan and Wu, 1995]:

$$CWF = \int_{z_0}^{z_T} \frac{g}{C_p T(z)} \frac{\eta}{1 + \gamma} [h(z) - \tilde{h}^*(z)] dz; \gamma = \frac{L}{C_p} \left(\frac{\partial \tilde{q}^*}{\partial T} \right)_p$$

where T , h , and q denote temperature, moist static energy, and water vapor mixing ratio, respectively. \tilde{h}^* and \tilde{q}^* are the saturation moist static energy and water vapor mixing ratio in the environment, outside of the cloud. g is gravitational acceleration, η is the mass flux, normalized by the cloud base value, C_p is heat capacity at constant pressure, and L is latent heat of vaporization. The integration is from z_0 to z_T , the cloud’s altitude range.

4. Analysis Procedure

[27] The analysis proceeded by the following steps:

[28] 1. The TRMM and MODIS data from August to October of 2000 and 2003 were matched and averaged in space and time, because the TRMM and MODIS satellite overpasses do not coincide perfectly. A 1° \times 1° grid and a time window ± 4 hours of the MODIS observations were used. The 1° \times 1° grid roughly accounts for spatial mismatch due to advection that takes place over a ± 4 hour time window. Anderson et al. [2003] have shown that over

Table 1. Linear Correlations Between Different Variables and Aerosol Optical Depth (τ_a) and Cloud Work Function (CWF)

Year	Variable	Correlation With τ_a			Correlation With CWF		
		R	p Value	95% Confidence Interval	R	p Value	95% Confidence Interval
2000	TMI rainfall	0.0876	0.000	0.0590–0.116	0.0602	0.000	0.0315–0.0888
2000	PR rainfall	0.151	0.000	0.102–0.200	0.0976	0.000	0.0476–0.147
2000	cloud top temperature	–0.128	0.000	–0.145 to –0.111	–0.125	0.000	–0.138 to –0.113
2000	cloud top pressure	–0.128	0.000	–0.145 to –0.110	–0.112	0.000	–0.124 to –0.0994
2000	cloud fraction	0.304	0.000	0.287–0.321	0.204	0.000	0.189–0.219
2000	% ice coverage	0.0717	0.000	0.0474–0.0959	0.135	0.000	0.119–0.151
2000	water path	0.254	0.000	0.205–0.302	0.0647	0.000	0.0371–0.0922
2003	TMI rainfall	0.0458	0.000	0.0230–0.0685	0.0749	0.000	0.0522–0.0976
2003	PR rainfall	0.0830	0.000	0.0419–0.124	0.0738	0.000	0.0326–0.115
2003	cloud top temperature	–0.0613	0.000	–0.0780 to –0.0445	–0.248	0.000	–0.259 to –0.237
2003	cloud top pressure	–0.0742	0.000	–0.0909 to –0.0574	–0.254	0.000	–0.265 to –0.243
2003	cloud fraction	0.282	0.000	0.266–0.297	0.205	0.000	0.192–0.218
2003	% ice coverage	0.0388	0.002	0.0148–0.0627	0.179	0.000	0.164–0.193
2003	water path	0.246	0.000	0.205–0.287	0.0847	0.000	0.0621–0.107

4 hours, the temporal autocorrelation of aerosol optical depth at a point location is still high (>0.8). We retained for analysis only $1^\circ \times 1^\circ$ grids where more than 10% of the grid area reported values, because the cloud variables (section 3.3) were retrieved only in cloud-covered pixels, and the lowest average cloud fraction was observed to be ~ 0.10 (see sections 5 and 6.4).

[29] 2. Control for synoptic forcing by dividing the data into different ranges of cloud work function (CWF), derived from the NCEP Reanalysis fields.

[30] 3. Examine relationships between aerosol optical depth versus precipitation and clouds, stratified by different bins of CWF .

5. Results

[31] We first examine simple linear correlations between τ_a and CWF versus rainfall and cloud variables to probe the potential existence of statistical relationships (Table 1). Almost all the variables exhibit highly significant correlations (R) with both τ_a and CWF ($p \ll 0.01$), the sole exception being the 2003 ice cloud coverage– τ_a relationship ($p = 0.02$). Correlation strengths of greater than 0.2 are found between cloud fraction and both τ_a and CWF , between WP and τ_a , and between cloud top temperature/pressure and CWF in 2003.

[32] Figures 2–5 plot the relationships of τ_a with rainfall and cloud properties for 2000 (left) and 2003 (right), stratified by different levels of CWF . The dotted, dashed, and solid lines range from the lowest to the top third of CWF , respectively. The data are binned by τ_a , with each bin spanning 20 percentile of the τ_a values. The error bars denote the standard errors (σ/\sqrt{N}) of the bin average. Each point in Figure 2 represents an average of ~ 310 $1^\circ \times 1^\circ$ grid cell values for TMI and a smaller number of ~ 90 values for PR, because of the PR's narrower swath. Approximately 770, 620, and 390 values are averaged in each point for cloud pressure/temperature, cloud fraction, and ice cloud coverage, respectively (Figures 3 and 4). The larger number compared to rainfall data follows from the fact that these variables were retrieved from the same satellite as τ_a , whereas rainfall observations derived from a separate platform (TRMM), thereby reducing overlap with τ_a observations. Each $\tau_a - CWF$ bin for WP (Figure 5) contains far fewer points (~ 100) because it was retrieved at 1 km \times

1 km footprint, and only pixels deemed to contain clouds yielded values.

[33] Increasing rainfall trends with τ_a can be seen in both years and both TRMM sensors (Figure 2), albeit the points displayed a fair amount of scatter and the increase was not monotonic. The increase was especially marked in the top two thirds of CWF in 2003 and in the 2000 TMI data. Rainfall is lower, in general, in the bottom third of CWF , as expected for conditions lacking buoyancy to generate convection. However, the rainfall– CWF relationship is far from straightforward, with the highest third of CWF not necessarily associated with the highest rainfall rates. In general, rainfall displayed correlations with CWF of less than 0.1 (Table 1). See section 6.3 for a discussion on CWF .

[34] The cloud top pressure and temperature exhibit clear relationships with τ_a (Figure 3), especially for higher levels of CWF . As τ_a is enhanced cloud top pressure and temperature both decrease, suggesting higher cloud tops. The fraction of surface area covered by clouds (“cloud fraction”) shows pronounced increases (Figure 4), from ~ 0.1 to greater than 0.3 as τ_a increases from 0.1 to greater than 0.5. In the presence of high CWF the increased cloud cover is particularly large, reaching fractions of over 0.4 in the highest τ_a bin. Concomitant with the enhanced cloud cover is the increased presence of ice clouds (Figure 4). Note that the “% ice cloud coverage” represents the percentage of $5 \text{ km} \times 5 \text{ km}$ pixels within the $1^\circ \times 1^\circ$ grid classified as ice phase; this differs from the cloud fraction, which was constructed using $1 \text{ km} \times 1 \text{ km}$ pixels from the cloud mask.

[35] WP also increases along with enhanced τ_a (Figure 5), suggesting that the column-integrated water (liquid + ice) increases from $\sim 80 \text{ g/m}^2$ at the lowest τ_a to values greater than $\sim 100 \text{ g/m}^2$ at the highest τ_a .

[36] We examined the statistical significance of relationships between τ_a and the variables shown in Figures 2–5, stratified by different groups of CWF . We adopted a nonparametric technique to be free from the Gaussian, constant-variance assumptions required by a classical technique like analysis of variance (ANOVA). Such assumptions can be violated by distinctly non-Gaussian variables such as rainfall and from heteroscedasticity stemming from variable retrieval and sampling errors dependent on atmospheric conditions. We used the Scheirer-Ray-Hare extension of the Kruskal-Wallis rank test [Sokal and Rohlf, 1994], which showed that for all variables except the 2000 ice

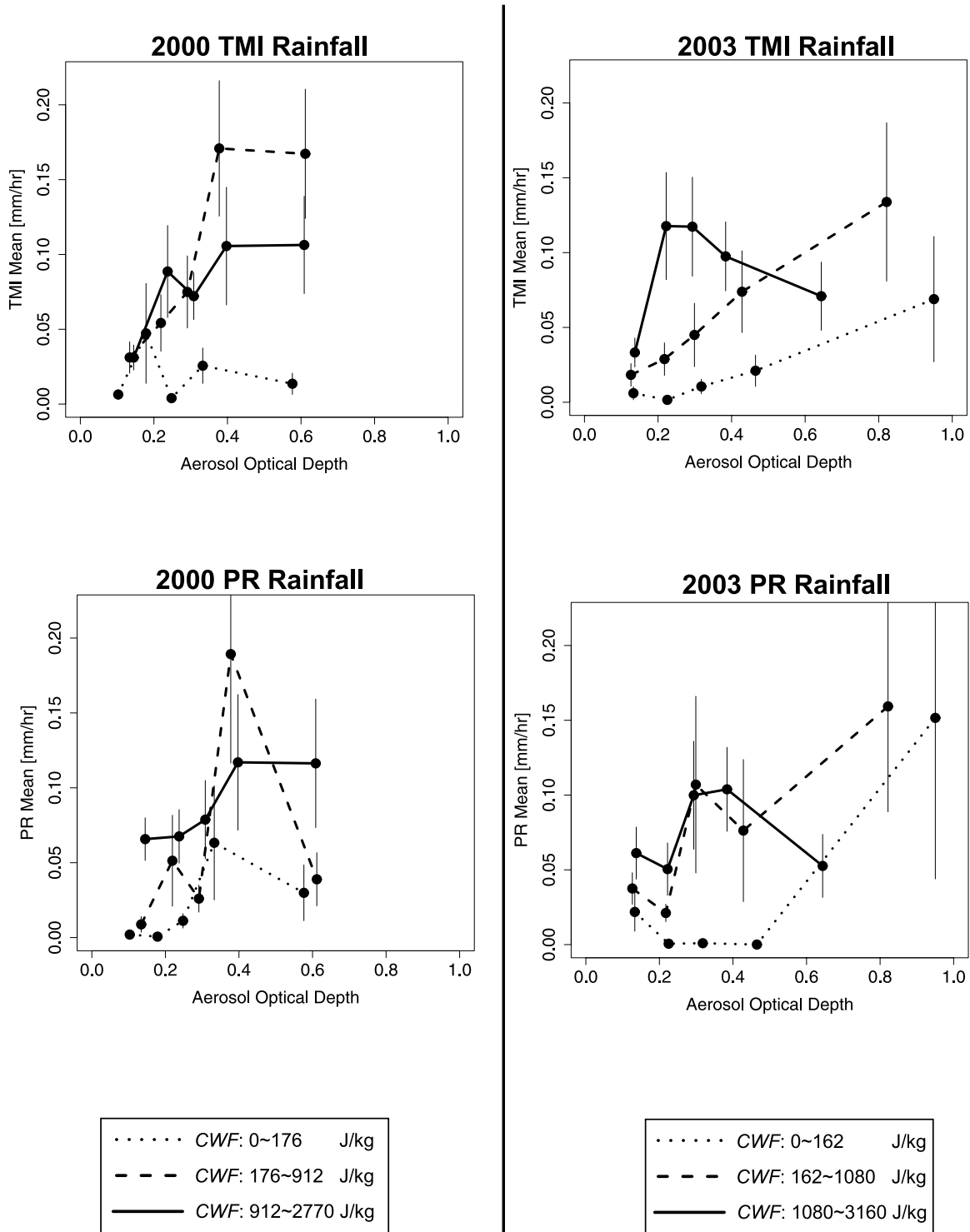


Figure 2. Relationships of TRMM rainfall measured by the TMI and PR sensors for (left) 2000 and (right) 2003 with MODIS aerosol optical depth (τ_a). The data are binned by τ_a , with each bin spanning 20 percentile of the τ_a values and further stratified into different *CWF* regimes. The dotted, dashed, and solid lines range from the lowest third to the top third values of *CWF*, respectively. The error bars denote the standard errors (σ/\sqrt{N}) of the bin average.

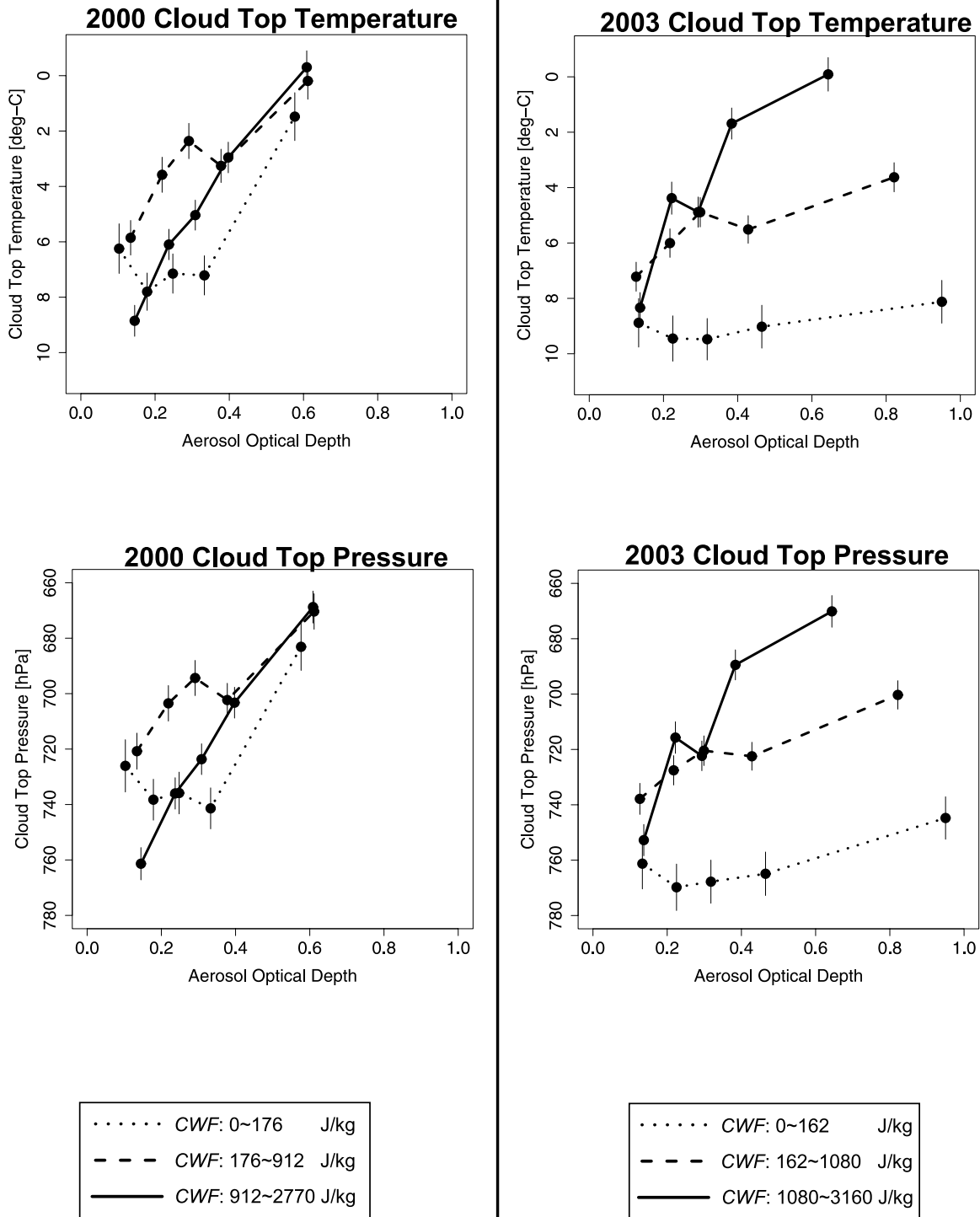


Figure 3. Same as Figure 2 but for (top) MODIS cloud top temperature and (bottom) pressure. Note the y axes have been inverted to indicate the fact that higher clouds are associated with lower cloud top temperatures/pressures.

cloud coverage, the null hypothesis of equivalent distributions under changing τ_a and CWF can be rejected at the $p < 0.01$ level. This suggests that the distributions of rainfall, cloud top pressure/temperature, cloud fraction, water path, and the 2003 ice cloud coverage are altered with changing

τ_a and CWF . The sole exception, ice cloud coverage in 2000, did not exhibit a highly significant relationship with CWF ($p = 0.026$). The “interaction term” between τ_a and CWF was also statistically significant ($p < 0.01$) for almost all variables (except for WP in 2000 and cloud fraction in

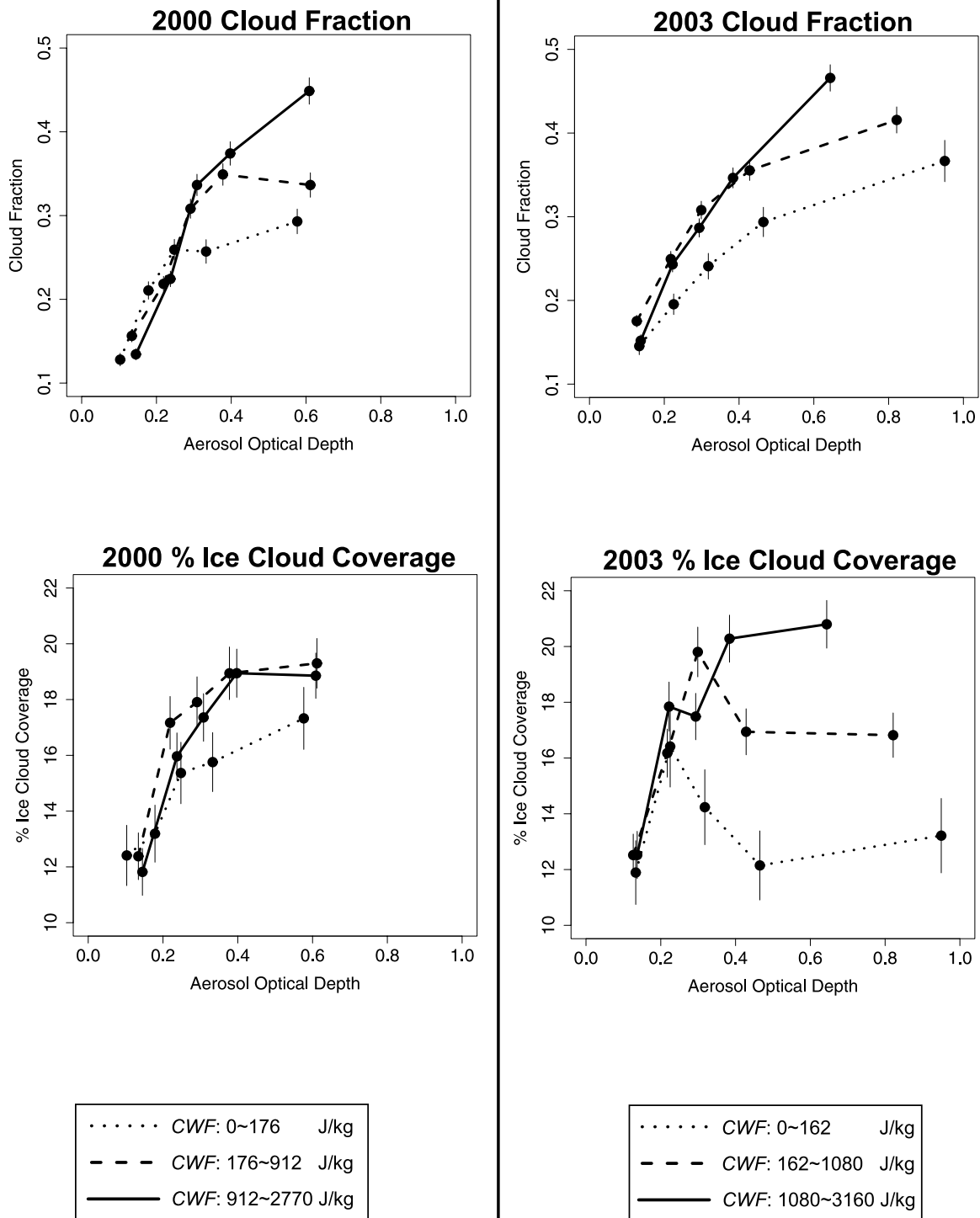


Figure 4. Same as Figure 2 but for (top) MODIS cloud fraction and (bottom) % ice coverage. Cloud fraction was calculated from the 1 km × 1 km cloud mask product, differing from ice coverage, which was derived from 5 km × 5 km pixels.

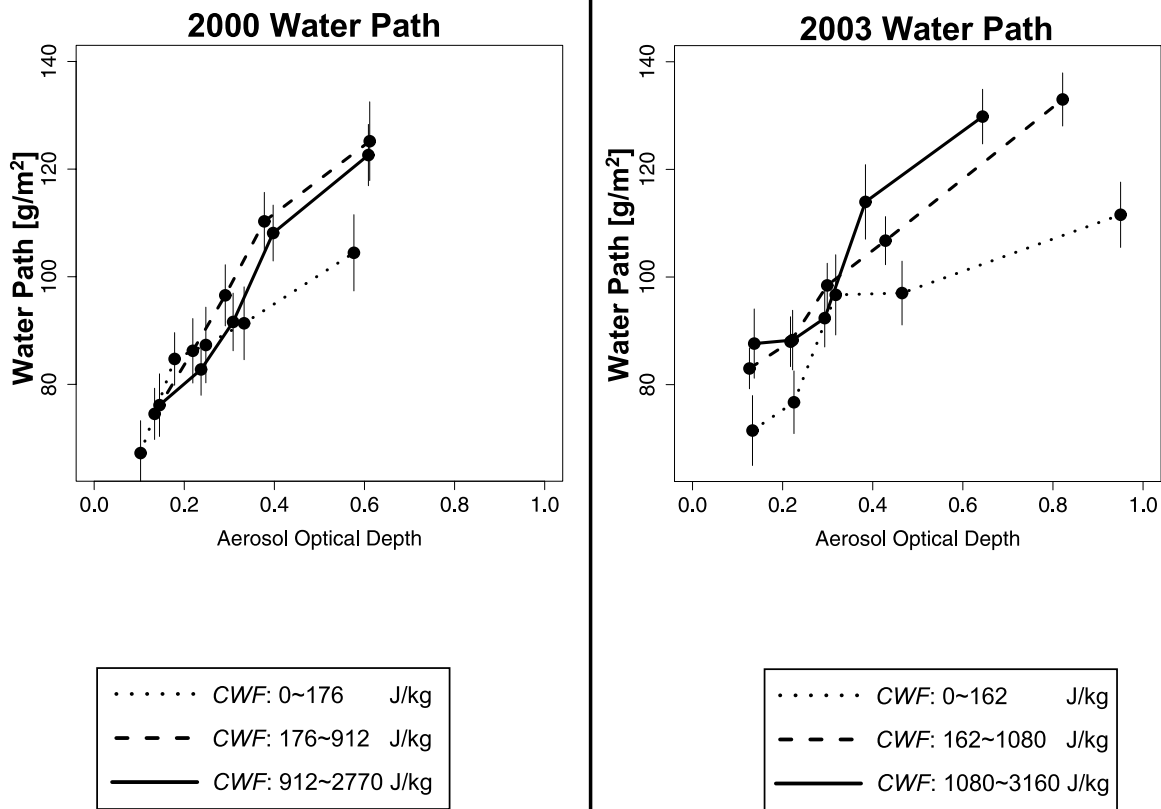


Figure 5. Same as Figure 2 but for MODIS water path.

2003), implying that the manner in which the distributions of these variables changed with τ_a depended on the CWF.

6. Discussion

6.1. Eliminating Potential Aerosol-Cloud Contamination

[37] Spurious correlations between τ_a and cloud properties can result if cloud retrievals were contaminated by presence of aerosols, or vice versa. Brennan et al. [2005] pointed out that contamination of cloud products began to take place at τ_a of ~ 0.6 . We have attempted to eliminate this contamination by removing pixels with the aerosol bit set to “true” in the cloud mask product from determination of cloud fraction, R_e , and WP , which should minimize contamination under thick smoke conditions (R. Frey, personal communication, 2005). Also, the cloud mask used by the aerosol retrieval [Martins et al., 2002] “automati-

cally rejects the first layer of non-cloudy pixels surrounding a cloud” [Koren et al., 2005, p. 4], thereby reducing the possibility for cloud contamination of the aerosol product.

[38] However, some residual misidentification of smoky pixels as clouds may persist. The misidentification may explain, for instance, the continued increases in cloud fraction at $\tau_a > 0.6$ in 2000 and 2003 (Figure 4). Nonetheless the trends with increased aerosol loading identified in this study clearly still hold for $\tau_a < 0.5$ (Figures 3–5): higher clouds, more extensive cloud cover, increased presence of ice clouds, and enhancement in WP .

6.2. Rainfall

[39] In this study higher τ_a is correlated with increases in Amazonian rainfall during the dry season (Figure 2). Although numerous researchers have suggested that warm-rain processes would be suppressed under aerosol loading [Albrecht, 1989; Ramanathan et al., 2001; Rosenfeld, 1999],

the impact on the net rainfall was unknown. Namely, if warm-rain processes were suppressed, it is not known whether subsequent cold-rain processes (ice phase) will be suppressed or not. Out of the previous studies only *Rosenfeld* [1999] specifically examined a combination of deep cumulus cloud and aerosols from biomass burning in the tropics, but this was a case study that only examined a single day rather than encompassing the entire burning season as was carried out here.

[40] A recent modeling study incorporating state-of-the-art spectral microphysics [*Khain et al.*, 2005] has shown that while elevated aerosol concentrations initially lead to lowered precipitation efficiency due to warm-rain suppression, dynamical feedbacks over the continent can actually result in enhanced rainfall. The delay in raindrop formation decreases the drag on updrafts by falling raindrops and increases the latent heat release by the additional water that reaches higher altitudes, where freezing takes place [*Khain et al.*, 2005]. The additional buoyancy generated by freezing has been hypothesized to be essential to deep convection in the Tropics [*Zipsler*, 2003]. Thus aerosols, by reducing drag and enhancing the release of latent heat from freezing, produce stronger vertical velocities over the continent and convergence in the boundary layer which can lead to squall lines and intense cold-rain processes [*Khain et al.*, 2005]. A similar result was observed in a simulation study using a general circulation model [*Lau et al.*, 2005].

[41] In fact, *Andreae et al.* [2004, p. 1341] reported anecdotal evidence of enhanced convection strength from biomass burning aerosols in the Amazon: “vigorous convection leading to intense thunderstorms and hail occurred in the smoky conditions... No reports of hail on the ground could be found for smoke-free conditions.”

[42] The hypothesis of aerosol-activated extreme thunderstorms and precipitation is consistent with observed distributions of nonzero rainfall rates from PR (Figure 6). The rainfall distributions show increased occurrence of events at the higher end of the distribution’s tail, with more extreme rainfall rates associated with increased levels of τ_a for both 2000 and 2003. Similar relationships were observed for TMI rainfall distributions (not shown).

[43] However, we note that microwave retrievals of rainfall over land are subject to large uncertainties. The large emissivity of the land surface obscures signals from hydrometeors reaching passive microwave sensors like the TMI [*Kummerow et al.*, 1996]. The TMI surface rainfall is therefore based upon a semiempirical relation between ice aloft and surface rainfall [*Wilheit et al.*, 2003]. The PR has good vertical resolution in the precipitation, but the single wavelength introduces uncertainties in the derived rainfall due to variable drop size distributions [*Masunaga et al.*, 2002]. Rainfall fall velocities, measured directly by neither TMI nor PR, introduces further uncertainties in rainfall estimates from both instruments [*Masunaga et al.*, 2002]. At the very least, we conclude that the TMI and PR, while observing somewhat different portions of the cloud, are both sensing the increased amount of hydrometeors in the atmosphere with τ_a , which is also verified by the MODIS *WP* observations (Figure 5).

[44] The uncertainties in the TRMM observations may account in part for the large scatter in the rainfall versus τ_a relationship in Figure 2. We underscore the fact that the

quantitative relationships established in Figures 2 and 6 are still very much preliminary and may be subject to future revisions when improved sensors and retrieval algorithms are available.

6.3. Correlation With Cloud Work Function

[45] While rainfall exhibits anticipated relationships with *CWF*, with lower rainfall clearly associated with stabler conditions, when *CWF* falls within the lowest-third bin (Figure 2), the correlation between *CWF* and rainfall is weak, with $R < 0.1$ in all cases (Table 1). The small statistical correlation may result from the coarse grid and time spacing ($2.5^\circ \times 2.5^\circ$, 6 hourly) of the NCEP Reanalysis that may fail to capture the subgrid-scale convective clouds that lead to precipitation. Also, errors in the Reanalysis moisture fields have been shown to be particularly large in the Tropics [*Mo and Higgins*, 1996; *Trenberth and Guillemot*, 1998]. Furthermore, a recent study has shown *CAPE*, closely related to *CWF* as a vertically integrated measure of buoyancy, to be uncorrelated with tropical rainfall on monthly timescales [*DeMott and Randall*, 2004]. These authors suggested the confounding effect of rainfall to destroy *CAPE* (opposing the role of *CAPE* in triggering rainfall) as a possible explanation.

[46] In summary, the Reanalysis-derived *CWF* may be an imperfect surrogate for the large-scale meteorological forcing for rainfall and convection. Hence the relationships between rainfall and cloud properties with aerosols observed in this study may still contain residual influences from meteorological forcing unaccounted by *CWF*.

6.4. Cloud Fraction and Height

[47] *Koren et al.* [2004] have reported a reduction in area covered by low-level scattered cumulus clouds over the Amazon, in apparent contrast to the increase in cloud fraction observed in this study (Figure 4). The discrepancy can be resolved by noting that all clouds detected by the satellite were included in this study’s consideration of “cloud fraction,” not just low-level scattered cumuli.

[48] Further, the combination of elevated cloud top height (Figure 3) and enhanced cloud cover suggests that the increased cloud cover took place primarily with cloud anvils rather than scattered cumuli. This is consistent with the invigoration of convection from aerosols. A similar increase in cloud cover and cloud top height correlated with τ_a was also observed by *Koren et al.* [2005] over the North Atlantic, on the basis of MODIS data. *Sekiguchi et al.* [2003] likewise reported clear, positive correlations in cloud cover and aerosol concentrations from AVHRR over the ocean.

[49] Concomitant with the enhanced cloudiness is an increased presence of ice clouds (Figure 4). This result follows from the elevated cloud top height to altitudes with lower temperatures and also supports the hypothesis of *Andreae et al.* [2004] that suggests aerosols could accelerate updrafts and lift cloud water to cold regions, where additional latent heat of freezing is released.

6.5. Water Path

[50] The increased *WP* in higher τ_a regimes may seem to corroborate *Albrecht* [1989], who also hypothesized this effect along with an increased cloud fraction. *Albrecht* [1989] observed, on the basis of one-dimensional modeling,

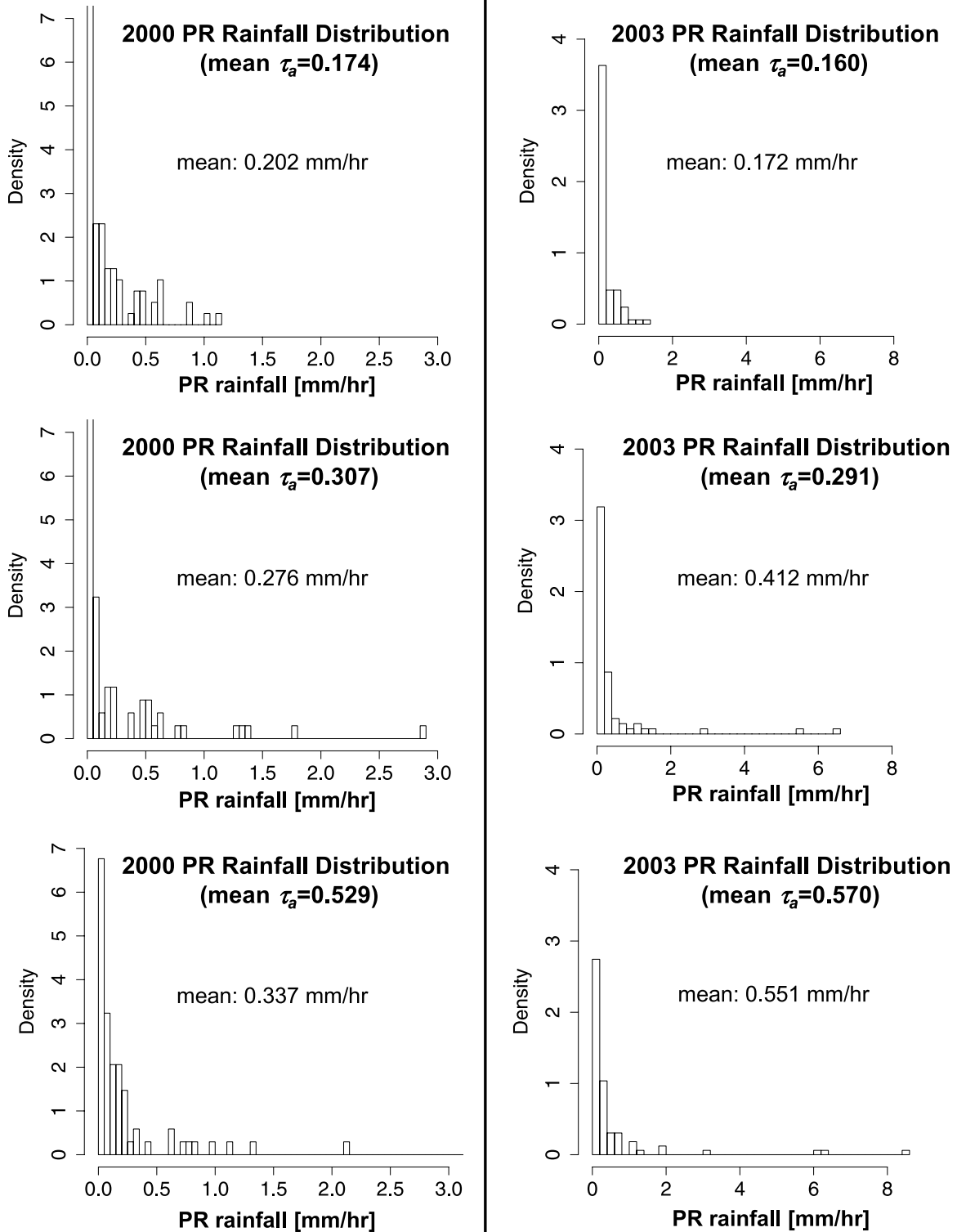


Figure 6. Probability density distributions of rainfall measured by the PR sensor for (left) 2000 and (right) 2003 at different levels of τ_a . The data were placed into three τ_a bins in each year. Only rainfall data with nonzero values and when *CWF* falls in the upper 50 percentile are plotted. Note that the axis ranges are different between the 2 years.

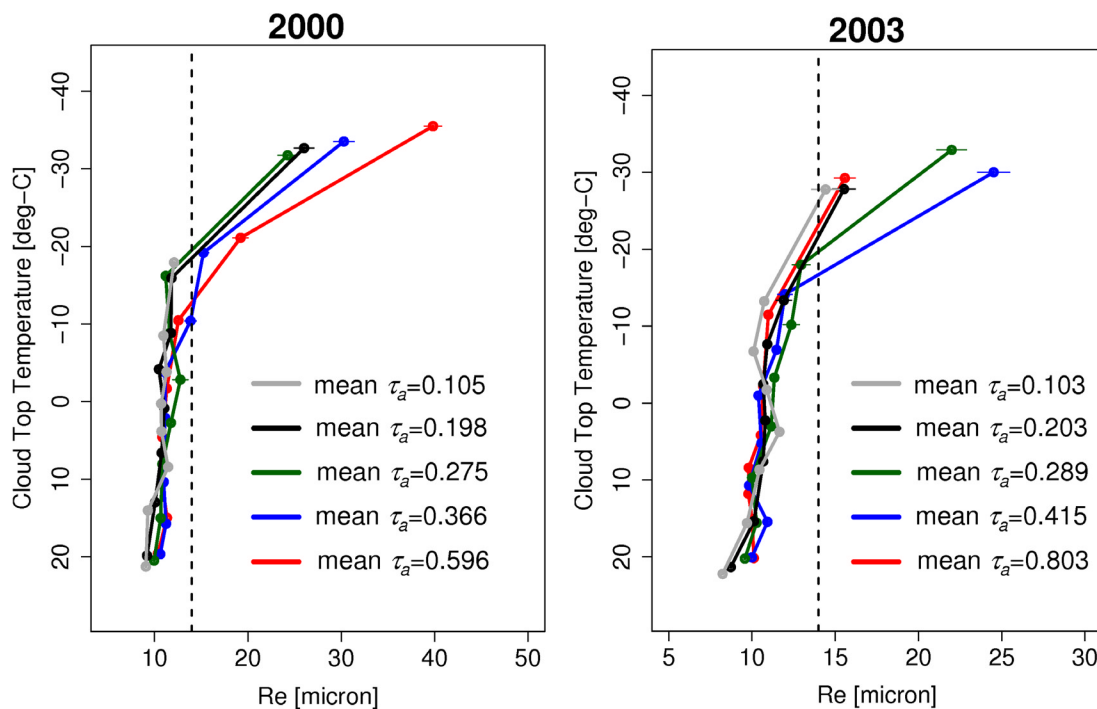


Figure 7. Cloud droplet effective radius (R_e) as a function of cloud top temperature, at different levels of aerosol optical depth (τ_a). The error bars denote the standard errors (σ/\sqrt{N}). The dotted line denotes the 14- μm threshold above which it has been suggested that hydrometeors reach sizes large enough to precipitate out of clouds [Rosenfeld and Gutman, 1994]. Note that the x axis changes between the years.

that aerosols decrease droplet sizes, reducing efficiency of drizzle and thereby enhancing cloud water and low-level cloudiness. The absence of total rainfall suppression seen in this study (Figure 2) does not preclude decreases in low-level drizzle if the precipitation originates at higher altitudes, from an aerosol-invigorated convection. However, contrary to the Albrecht [1989] prediction, shallow cumulus cloud cover decreases from biomass-burning-derived aerosols [Koren *et al.*, 2004] in the Amazon Basin. Thus the increase in total cloud fraction likely reflects increased cloud cover at higher altitudes, as mentioned in the previous section.

6.6. R_e -Cloud Top Temperature Relationships

[51] The relationship between R_e and cloud top temperature reveals microphysical processes taking place in clouds [Rosenfeld and Lensky, 1998]. The small increase in R_e with cloud height at temperatures greater than freezing, at lower parts of the atmosphere (cloud top temperature $> -10^\circ\text{C}$), reflects diffusional growth [Rosenfeld and Lensky, 1998]. The steep dR_e/dT slope at higher altitudes (cloud top temperature $< -10^\circ\text{C}$) indicates droplet coalescence and especially the formation of ice, forming a “mixed phase zone.” Figure 7 shows this relationship, averaged for the 2 years, at different levels of τ_a . The dotted line denotes the 14- μm threshold above which it has been suggested that hydrometeors reach sizes large enough to precipitate out of clouds [Rosenfeld and Gutman, 1994].

[52] At background aerosol levels ($\tau_a = 0.1$) the average R_e profile did not increase beyond the 14- μm precipitation

threshold in 2000 and barely crossed the threshold in 2003. Differences in R_e growth between various levels of τ_a were found at temperatures below -10°C , in the mixed phase zone. No clear mixed phase zone was found at background aerosol levels, while sharp increases in R_e with decreasing temperature, indicative of ice formation, was observed at higher τ_a , especially in 2000. In 2000 this “mixed phase zone” [Rosenfeld and Lensky, 1998] formed at progressively lower cloud top temperatures with elevated τ_a : at the highest τ_a level the mixed phase zone was elevated to altitudes with temperatures $\sim -20^\circ\text{C}$ in 2000. Ice phase formation and release of latent heat in the mixed phase zone lead to higher cloud tops at aerosol levels elevated above the background, as already seen in Figure 3.

[53] The decrease in R_e associated with biomass burning, previously observed by Kaufman and Fraser [1997] in the Amazon and Rosenfeld [1999] in Indonesia, appears to be manifested slightly only at the highest level of τ_a in 2003. Perhaps the same reduction in R_e was not seen in 2000 because τ_a was not as high, and the composite relationship in Figure 7 aggregates data from all regions, with different clouds together, rather than restricting the analysis to limited spatial regions as conducted by Rosenfeld [1999]. Moreover, Kaufman and Fraser [1997] only analyzed low (cloud top temperature $\geq -3^\circ\text{C}$) clouds, whereas this analysis pooled observations of all cloud types.

[54] The lack of a clear decrease in R_e may also reflect nonmicrophysical mechanisms that invigorate convection. Andreae *et al.* [2004] proposed that the heat from forest

fires can strengthen updrafts. Secondly, aerosol absorption of sunlight causes diabatic heating in the boundary layer and has the potential to cause stronger convective events and increase both *WP* and cloud fraction, as Feingold *et al.* [2005] demonstrated in a detailed large eddy simulation of smoke-cloud interactions, albeit the same study showed these results to depend on the altitude of the aerosol layer relative to the cloud height. Rudich *et al.* [2003] also suggested that absorption of solar radiation by aerosols induced convection and cloud formation, based on empirical observations of Middle Eastern oil fires.

7. Summary and Conclusions

[55] On the basis of an empirical analysis of satellite observations, this study examined correlations between aerosol loading (primarily from biomass burning) and rainfall and cloud properties in the Amazon Basin, during the dry season. While this work cannot unequivocally establish causal links between aerosols and the observed changes, the analysis revealed the following correlations associated with increased aerosols that need to be reproduced in future modeling studies: (1) increased precipitation, (2) increased occurrence of intense rainfall events, (3) enhanced cloud cover, (4) elevated cloud tops, (5) increased water path, and (6) greater formation of ice.

[56] The aforementioned results are in accordance with the hypothesis proposed by Andreae *et al.* [2004] for the Amazon. This hypothesis suggests that aerosols from biomass burning would invigorate convection by drawing upon heat from the fires as well as by delaying onset of precipitation until higher altitudes, where formation of ice hydrometeors rather than warm rain releases greater latent heat. The greater vigor of storms could explain the increases in precipitation, cloud height, and cloud cover seen in this study.

[57] The observed changes in rainfall and cloud properties are likely to have major climate impacts in the Amazon Basin. We present a qualitative discussion below rather than attempt an exact quantitative assessment of these climate impacts, because of the simple correlative nature of this study, uncertainties in rainfall retrievals (section 6.2), and potential incomplete accounting for meteorological forcing using the *CWF* (section 6.3).

[58] The changes in cloud properties are likely to significantly affect the Amazon's radiative budget. The increase in total cloud cover may partially counteract the positive shift in radiative forcing caused by reduction in shallow clouds as reported by Koren *et al.* [2004]. However, the concomitant shift to elevated cloud tops would also have radiative consequences. We defer the quantitative determination of radiative forcing to a future study that incorporates detailed radiative transfer calculations.

[59] If the enhanced rainfall due to biomass burning is indeed occurring, the additional precipitation taking place during the dry season can have important societal [*IPCC*, 2001a] and biogeochemical [*Saleska et al.*, 2003] consequences. The accelerated burning in the Amazon for agricultural land use over the past several decades [*Crutzen and Andreae*, 1990; *Setzer et al.*, 1994] and the associated enhancements in aerosols and rainfall may even partly account for the observed multidecadal positive trend in

Amazonian precipitation [*Chen et al.*, 2001; *Easterling et al.*, 2000].

[60] **Acknowledgments.** We thank D. Rosenfeld, C. Castro, H. Masunaga, and W. Berg for helpful discussions and extend our gratitude to the entire MODIS team (especially R. Frey, S. Platnick, and A. Chu) for making available the MODIS products and for explaining technical details regarding the products. We acknowledge support from NASA (grants NNG04GB87G and NNG04GL61G). J.C.L. was supported by the NOAA Postdoctoral Program in Climate and Global Change, administered by the University Corporation for Atmospheric Research.

References

- Ackerman, S., et al. (2002), Discriminating clear-sky from cloud with MODIS, Algorithm Theoretical Basis Document, 112 pp., NASA Goddard Space Flight Cent., Greenbelt, Md.
- Ackerman, S. A., et al. (1998), Discriminating clear sky from clouds with MODIS, *J. Geophys. Res.*, *103*(D24), 32,141–32,157.
- Albrecht, B. A. (1989), Aerosols, cloud microphysics, and fractional cloudiness, *Science*, *245*(4923), 1227–1230.
- Anderson, T. L., et al. (2003), Mesoscale variations of tropospheric aerosols, *J. Atmos. Sci.*, *60*(1), 119–136.
- Andreae, M. O., et al. (2004), Smoking rain clouds over the Amazon, *Science*, *303*, 1337–1342.
- Arakawa, A., and W. H. Schubert (1974), Interaction of a cumulus cloud ensemble with the large-scale environment. Part I, *J. Atmos. Sci.*, *31*, 674–701.
- Brennan, J. I., et al. (2005), Aerosol-cloud interaction—Misclassification of MODIS clouds in heavy aerosol, *IEEE Trans. Geosci. Remote Sens.*, *43*(4), 911–915.
- Chahine, M. T. (1992), The hydrological cycle and its influence on climate, *Nature*, *359*, 373–380.
- Chen, T.-C., et al. (2001), Suppressing impacts of the Amazonian deforestation by the global circulation change, *Bull. Am. Meteorol. Soc.*, *82*(10), 2209–2216.
- Chu, D. A., Y. J. Kaufman, C. Ichoku, L. A. Remer, D. Tanré, and B. N. Holben (2002), Validation of MODIS aerosol optical depth retrieval over land, *Geophys. Res. Lett.*, *29*(12), 8007, doi:10.1029/2001GL013205.
- Crutzen, P. J., and M. O. Andreae (1990), Biomass burning in the tropics: Impact on atmospheric chemistry and biogeochemical cycles, *Science*, *250*, 1669–1678.
- DeMott, C. A., and D. A. Randall (2004), Observed variations of tropical convective available potential energy, *J. Geophys. Res.*, *109*, D02102, doi:10.1029/2003JD003784.
- Easterling, D. R., et al. (2000), Observed climate variability and change of relevance to the biosphere, *J. Geophys. Res.*, *105*(D15), 20,101–20,114.
- Emanuel, K. A. (1994), *Atmospheric Convection*, Oxford Univ. Press, New York.
- Feingold, G., H. Jiang, and J. Y. Harrington (2005), On smoke suppression of clouds in Amazonia, *Geophys. Res. Lett.*, *32*, L02804, doi:10.1029/2004GL021369.
- Food and Agriculture Organization (1993), Third interim report on the state of tropical forests, Rome.
- Guyon, P., et al. (2003), Physical properties and concentration of aerosol particles over the Amazon tropical forest during background and biomass burning conditions, *Atmos. Chem. Phys.*, *3*, 951–967.
- Hartmann, D. L. (1994), *Global Physical Climatology*, 411 pp., Elsevier, New York.
- Iguchi, T., et al. (2000), Rain-profiling algorithm for the TRMM precipitation radar, *J. Appl. Meteorol.*, *39*, 2038–2052.
- Intergovernmental Panel on Climate Change (2001a), *Climate Change 2001: Impacts, Adaptation and Vulnerability*, 1000 pp., Cambridge Univ. Press, New York.
- Intergovernmental Panel on Climate Change (2001b), *Climate Change 2001: The Scientific Basis*, 944 pp., Cambridge Univ. Press, New York.
- Kalnay, E., et al. (1996), The NCEP/NCAR 40-year reanalysis project, *Bull. Am. Meteorol. Soc.*, *77*(3), 437–471.
- Kaufman, Y. J., and R. S. Fraser (1997), The effect of smoke particles on clouds and climate forcing, *Science*, *277*, 1636–1639.
- Kaufman, Y. J., and D. Tanre (1998), Algorithm for remote sensing of tropospheric aerosol from MODIS, 85 pp., NASA Goddard Space Flight Cent., Greenbelt, Md.
- Kaufman, Y. J., et al. (1997), Operational remote sensing of tropospheric aerosol over the land from EOS-MODIS, *J. Geophys. Res.*, *102*, 17,051–17,068.
- Khain, A., D. Rosenfeld, and A. Pokrovsky (2005), Aerosol impact on the dynamics and microphysics of deep convective clouds, *Q. J. R. Meteorol. Soc.*, *131*, 1–25.

- Kidder, S. Q., and T. H. Vonder Haar (1995), *Satellite Meteorology: An Introduction*, 466 pp., Elsevier, New York.
- King, M. D., et al. (1997), Cloud retrieval algorithms for MODIS: Optical thickness, effective particle radius, and thermodynamic phase, 79 pp., NASA Goddard Space Flight Cent., Greenbelt, Md.
- Koren, I., et al. (2004), Measurement of the effect of Amazon smoke on inhibition of cloud formation, *Science*, *303*, 1342–1345.
- Koren, I., et al. (2005), Aerosol invigoration and restructuring of Atlantic convective clouds, *Geophys. Res. Lett.*, *32*, L14828, doi:10.1029/2005GL023187.
- Kummerow, C., W. S. Olson, and L. Giglio (1996), A simplified scheme for obtaining precipitation and vertical hydrometeor profiles from passive microwave sensors, *IEEE Trans. Geosci. Remote Sens.*, *34*(5), 1213–1232.
- Kummerow, C., et al. (2000), The status of the Tropical Rainfall Measuring Mission (TRMM) after two years in orbit, *J. Appl. Meteorol.*, *39*, 1965–1982.
- Lau, K. M., et al. (2005), Effects of cloud microphysics on tropical atmospheric hydrologic processes and intraseasonal variability, *J. Clim.*, *18*, 4731–4751.
- Laurance, W. F., and G. B. Williamson (2001), Positive feedbacks among forest fragmentation, drought, and climate change in the Amazon, *Conservation Biol.*, *15*(6), 1529–1535.
- Lohmann, U., and J. Feichter (2005), Global indirect aerosol effects: A review, *Atmos. Chem. Phys.*, *5*, 715–737.
- Martins, J. V., D. Tarré, L. Remer, Y. Kaufman, S. Mattoo, and R. Levy (2002), MODIS Cloud screening for remote sensing of aerosols over oceans using spatial variability, *Geophys. Res. Lett.*, *29*(12), 8009, doi:10.1029/2001GL013252.
- Masunaga, H., T. Iguchi, and R. Oki (2002), Comparison of rainfall products derived from TRMM Microwave Imager and Precipitation Radar, *J. Appl. Meteorol.*, *41*, 849–862.
- Menzel, P., et al. (2002), Cloud top properties and cloud phase, Algorithm Theoretical Basis Document, 61 pp., NASA Goddard Space Flight Cent., Greenbelt, Md.
- Mo, K., and R. W. Higgins (1996), Large-scale atmospheric moisture transport as evaluated in the NCEP/NCAR and the NASA/DAO reanalyses, *J. Clim.*, *9*, 1531–1545.
- National Research Council (2005), *Radiative Forcing of Climate Change: Expanding the Concept and Addressing Uncertainties*, Natl. Acad. Press, Washington, D. C.
- Nicholson, S. E., et al. (2003), Validation of TRMM and other rainfall estimates with a high-density gauge dataset for West Africa. Part II: Validation of TRMM rainfall products, *J. Appl. Meteorol.*, *42*, 1355–1368.
- Pan, H.-L., and W.-S. Wu (1995), Implementing a mass flux convection parameterization package for the NMC medium-range forecast model, *NMC Off. Note*, *409*, 40 pp., Natl. Cent. for Environ. Predict., Camp Springs, Md.
- Platnick, S. (2000), Vertical photon transport in cloud remote sensing problems, *J. Geophys. Res.*, *105*(D18), 22,919–22,935.
- Platnick, S., et al. (2003), The MODIS cloud products: Algorithms and examples from Terra, *IEEE Trans. Geosci. Remote Sens.*, *41*(2), 459–473.
- Procopio, A. S., P. Artaxo, Y. J. Kaufman, L. A. Remer, J. S. Schafer, and B. N. Holben (2004), Multiyear analysis of Amazonian biomass burning smoke radiative forcing of climate, *Geophys. Res. Lett.*, *31*, L03108, doi:10.1029/2003GL018646.
- Ramanathan, V., et al. (2001), Aerosols, climate, and the hydrological cycle, *Science*, *294*, 2119–2124.
- Remer, L. A., et al. (2005), The MODIS aerosol algorithm, products and validation, *J. Atmos. Sci.*, *62*, 947–973.
- Rosenfeld, D. (1999), TRMM observed first direct evidence of smoke from forest fires inhibiting rainfall, *Geophys. Res. Lett.*, *26*(20), 3105–3108.
- Rosenfeld, D., and G. Gutman (1994), Retrieving microphysical properties near the tops of potential rain clouds by multispectral analysis of AVHRR data, *J. Atmos. Res.*, *34*, 259–283.
- Rosenfeld, D., and I. M. Lensky (1998), Satellite-based insights into precipitation formation processes in continental and maritime convective clouds, *Bull. Am. Meteorol. Soc.*, *79*(11), 2457–2476.
- Rudich, Y., A. Sagi, and D. Rosenfeld (2003), Influence of the Kuwait oil fires plume (1991) on the microphysical development of clouds, *J. Geophys. Res.*, *108*(D15), 4478, doi:10.1029/2003JD003472.
- Saleska, S. R., et al. (2003), Carbon in Amazon forests: Unexpected seasonal fluxes and disturbance-induced losses, *Science*, *302*, 1554–1557.
- Sekiguchi, M., et al. (2003), A study of the direct and indirect effects of aerosols using global satellite data sets of aerosol and cloud parameters, *J. Geophys. Res.*, *108*(D22), 4699, doi:10.1029/2002JD003359.
- Setzer, A. W., M. C. Pereira, and A. C. Pereira Jr. (1994), Satellite studies of biomass burning in Amazonia—Some practical aspects, *Remote Sens. Rev.*, *10*, 91–103.
- Simpson, J., et al. (1996), On the Tropical Rainfall Measuring Mission (TRMM), *Meteorol. Atmos. Phys.*, *60*, 19–36.
- Sokal, R. R., and F. J. Rohlf (1994), *Biometry*, 880 pp., W. H. Freeman, New York.
- Trenberth, K. E., and C. J. Guillemot (1998), Evaluation of the atmospheric moisture and hydrological cycle in the NCEP/NCAR reanalyses, *Clim. Dyn.*, *14*, 213–231.
- Twomey, S. (1977), The influence of pollution on the shortwave albedo of clouds, *J. Atmos. Sci.*, *34*, 1149–1152.
- Warner, J., and S. Twomey (1967), The production of cloud nuclei by cane fires and the effect on cloud droplet concentration, *J. Atmos. Sci.*, *24*, 704–706.
- Wilheit, T., C. Kummerow, and R. Ferraro (2003), Rainfall algorithms for AMSR-E, *IEEE Trans. Geosci. Remote Sens.*, *41*(2), 204–214.
- Zipser, E. J. (2003), Some views on “hot towers” after 50 years of tropical field programs and two years of TRMM data, in *Cloud Systems, Hurricanes, and the Tropical Rainfall Measuring Mission (TRMM)*, edited by W.-K. Tao and R. Adler, *Meteorol. Monogr.*, *29*(51), 49–58.

C. Kummerow, T. Matsui, and R. A. Pielke Sr., Department of Atmospheric Science, Colorado State University, Fort Collins, CO 80523-1371, USA.

J. C. Lin, Department of Earth Sciences, University of Waterloo, 200 University Avenue West, Waterloo, ON, Canada N2L 3G1. (jcl@uwaterloo.ca)